# A Topological Study of a Surface Signaling Network with Relevance to Brain Function


## Authors

Siddhartha Sen[1]*, Tomás J. Ryan[2,3,4], David Muldowney[1], and Maurizio Pezzoli[5.]

## Affiliations

1. School of Physics, Trinity College Dublin, Ireland.
2. School of Biochemistry and Immunology and Trinity College Institute of Neuroscience, Trinity College Dublin, Ireland.
3. Florey Institute of Neuroscience and Mental Health, Melbourne Brain Centre, University of Melbourne, Victoria, Australia.
4. Child & Brain Development Program, Canadian Institute for Advanced Research (CIFAR), Toronto, Ontario, Canada.
5. Brain Mind Institute, School of Life Sciences, École Polytechnique Fédérale de Lausanne, Switzerland

* Corresponding Author, contact: sen1941@gmail.com



## Abstract

In this paper we construct a mathematical surface-network where topological changes of the network are linked to signal generating events within it. The surface nature of the network is used to show how changes to a set of topological parameters of a subsystem of the network, produced by local geometric deformations, generate output traveling signals and that these signals carry with them the topological and geometric deformation parameter values that created them. In this scheme, topological architectural information of this subsystem and traveling signals are mathematically linked. We suggest that the possibility of such a theoretical link between a system's topology and the signals it produces could have major implications in our understanding of biological networks, such as the brain.


## Main Text

## Introduction

The brain can be observed throughout the animal kingdom as a self-assembled autonomous signaling network. A range of connectome solutions exists to process sensorial information and generate relevant behavioral responses to the environment. Although there is no agreed view about a common evolutionary ancestral origin of complex neural networks[1,2], there exists a vast number of possible arrangements of cell types with different composition of neurotransmitters and microcircuits performing different tasks. However, this complex assembly is organized so that it

operates as a single coherent unit[3]. How is it possible that a diaspora of different neural assembles, converges into a signaling network with a self-interpretating coding system?

For such an autonomous system to function, a common link must exist between the structure and the signaling code. Through a formal mathematical system, we present a possible way to address this issue, by showing that both structure and signal can be complementary aspects of the same object. By mathematical means we establish how a coherence is possible by correlating input information introduced to a subunit of a network, here treated as topological deformations induced by local geometric means, with the generation of signals that carry with them this topological and geometric information. The aim of this paper is to search for some latent rules on how an autonomous signaling network could be built.

Conceptually, our approach is holistic. We construct a mathematical framework where basic universal features for an electroconductive network are assigned, while leaving its geometric architecture features with as much freedom as possible.

We define our network as an electroconductive surface, one that can be pictured as covering any three-dimensional, branch-like manifold. It can be understood as a sort of reticular configuration of connected tubes. The surface nature of the presented network permits us to simplify the study by the use of the mathematical discipline of topology[4,5] for the analysis. In this discipline two objects that can be continuously deformed into each other are regarded as the same. For instance, the surface of a sphere is equivalent to that of an ellipsoid.

Since our network is a surface, its dynamics are defined by laws that decide how special input surface deformations lead to output signals as responses. We further require that the surface-network is smooth, then a mathematical result tells us[5] that it can be parametrized by algebraic equations. We will show that if our surface network is parametrized by a specific algebraic equation and has an additional layer of topological structure that makes it have electroconductive properties, then signal generation induced by topology changes is possible.

## THE FRAMEWORK

We next present a mathematical object that attempts to describe an electroconductive, signaling surface network The approach shows how signal generation can be a global process involving transient topology changes to its subunits. The surface itself can be pictured as a two-dimensional cover of a complex converging and diverging network, with branchlike three-dimensional architecture. Our analysis of the surface uses the ideas of topological connectivity[4,6].

Certain restrictions on the nature of the surface must be added for the sake of providing a proper network description. First, it must be orientable. This means that the surface has two sides. Second, the surface has to have topological connectivity properties. This means it contains a multitude of tubes joined together, in different regions, to form a connected surface without boundaries. The topological classifying theorem for surfaces[6], tells us that any surface without boundaries, no matter how complex, constructed as described, can always be rearranged to look like a sphere with *g* tubes attached or as a set of connected *g* donuts (tori) surfaces (Fig 1). The number of donuts or the number of surface tubes on a sphere is called the genus or genus number of the surface. It is fixed by the form of the algebraic equation that parametrizes the surface. Ours is a surface of high genus number. The surface of a sphere has a genus 0, the surface of a torus has a genus 1, our surface has then a genus *g* (Fig 1A).

We suppose our surface network is smooth. This allows us use ideas of surface calculus in our analysis[7]. Then, such a network can be described by using topological coordinates that are a set of special 2*g* closed loops ($a_1, a_2, \ldots a_g; b_1, b_2, \ldots b_g$).

A two-dimensional, orientable smooth surface of the kind described is called a Riemann Surface. (App. I).

The set of topological loop coordinates are geometrical objects that provide a representation of the connectivity features of the Riemann Surface. While the smoothness of a Riemann Surface of genus *g* $\sum_g$ , is represented by a set of *g* smooth one-forms[6]. One-forms are objects that can be integrated along one-dimensional loops or paths (App. II).

These two sets of mathematical objects that describe a Riemann Surface can be used to introduce a set of variables, which in turn can be used to define a natural algebraic function that represents the Riemann Surface. The algebraic variables are obtained by simply integrating the set of *g* smooth one-forms over the set of 2*g* loop coordinates of $\sum_g$ to produces a set of 2*g* numbers, or integrated over paths with a fixed starting point and a variable point *z* of the Riemann Surface to generate a set of *g* variable points. Smooth one-forms are called holomorphic differential one-forms (App. II A).

We write holomorphic or smooth one-forms as, $\omega_i(u)du$. Smoothness means that the functions that multiply $du$ can be differentiated an arbitrary number of times with respect to the complex variable $u$. The *g* one-forms as well as the 2*g* loops topological coordinates, necessary to describe our surface-network, a Riemann Surface of genus *g*, can be constructed using the mathematical result that all Riemann Surfaces can be parameterized by polynomial algebraic equations in terms of two complex variables[5] (App. I). In our case the relevant algebraic equation is called a real hyperelliptic equation. This equation parametrizes our surface network.

A real hyperelliptic equation for a genus *g* Riemann Surface is defined by,

$$y^2(u) = \prod_{i=1}^{2g+2}(u - a_i)$$

$$= P(u)$$

Where $u, y$ are complex numbers but $a_i,\ i = 1, 2, \ldots (2g + 2)$ are either all real numbers or they occur as a pair of complex conjugate numbers. The way to construct our genus *g* Riemann $\sum_g$ from this equation is described (App. III).

To make our surface electroconductive we next introduce charges on $\sum_g$ as surface electrons. This step introduces a new topological feature to the surface, namely, a topological spin structure. This is because the electrons are spin half particles that have magnetic properties which allows them to form different topologically inequivalent patterns[8, 9].

Our surface network now has electroconductive properties as electrons carry charge, while at the mathematical level it has two layers of topology: one reflecting its topological connectivity, given by its non-zero genus ($g > 0$) and the other from the presence of surface electrons, that gives the system a spin structure. These two topological properties have associated with them topological numbers. Thus, the topologically distinct arrangements of linked surface electron spins carry a topological charge number *W*, which we will discuss later, while the connectivity topology of the surface is given by its genus *g*. Since the surface is now charged, all local topological surface distortions will generate local voltage variations (App. IV).

Thus, to summarize, we have described an electroconductive surface network, a special Riemann Surface of genus *g* ($\sum_g$ ) with spin structure that has topological properties that are given by two numbers (*g*, *W*), which is parametrized by a real hyperelliptic equation.

## LOCAL TOPOLOGICAL DISTORTIONS

We now make our $\sum_g$ into a dynamical system by introducing a dynamical law that defines the nature of allowed input signals to the system and then determines the system's response to them. Our dynamical law states that both the input signals and responses to them must respect the mathematical properties of the Riemann Surface network. Keeping this requirement in mind we define input signals, local deformations, in terms of objects that are well defined on a Riemann Surface (App. II A). But before this can be done, we will have to introduce some mathematical ideas and explain the geometric nature of the input signal, a pinch deformation, in terms of Riemann Surface variables. Later we will show how the dynamical law also determines the nature of responses to pinch deformations.

A pinch deformation input signal, is a local geometric distortion of the surface that reduces the circumference of a loop $a_i$ at a point to zero (Fig 2A). It is the universal input signal of the network. Such a deformation also changes the topology of the subunit in which it occurs and initiates charge movement (App. IV).

To describe the dynamics of these geometrical deformations to the Riemann Surface we need to introduce an appropriate algebraic function. Then, we show, a geometric pinch can be described in algebraic terms. To do this we use the natural variables of the Riemann Surface. Since a pinch deformation corresponds to reducing a circumference of a $a_i$ loop at a point, an algebraic description of this process can be obtained by taking the loop integral of a one-form along the loop that is getting deformed. As the loop shrinks to zero, we now have an algebraic representation with deformation parameters of the process in terms of the natural variables of the Riemann Surface (App. II B).

Such a pinch deformation reduces the circumference of a single $a_i$ loop at a point to zero, thus transiently reducing the genus of $\sum_g$ from $g$ to $g$ - 1.

## NODE EVENT

We explained how a natural set of deformation parameters that identify the nature of pinch deformation input signal can be introduced (App. II B). A set of simultaneous pinch deformations of a subunit of $\sum_g$ of genus $k < g$ ($\sum_k$ ), that reduce these topological numbers of the subunit to zero, creates a transient topological sphere (Fig 2B). We define this process as a node event.

We next explain how the response of the surface network to such pinch inputs can be obtained from the dynamical law. In this case, the dynamical law can be viewed as a compatibility condition. To proceed we next use the fact that the algebraic function used to describe the $\sum_g$ is valid only if the function satisfies a nonlinear constraint[10]. Under pinch deformations that we consider, this nonlinear constraint becomes a set of nonlinear differential equations, known as the nonlinear Schrödinger differential equations[11]. Thus, the dynamical law requires that the response functions to pinch deformations must be solutions of these equations for the responses to be compatible with the mathematical Riemann Surface structure.

We now have a dynamic input-output set up for our surface network, where local pinch deformations are input signals that produce output pulses that are solutions of a set of nonlinear Schrödinger differential equations. This scheme of signal generation is established, not on the basis of observational inputs, but from a mathematical analysis of compatibility that exploits the topological features of the special electroconductive surface network.

We observe that as pinch deformations reduce the circumferences of a set of $k$ $a_i$ loops to zero, they transiently reduce the genus of $\sum_k$ from its genus value $k$ to zero which also reduces its

topological spin structure charge *W*, to zero. Since our surface is charged, these distortions will generate local voltage variation pulse signals (App. IV B and VII) that carries away the topological numbers of the network as well as the pinch deformation details with them.

We have described the properties of $\sum_g$ that we use for our surface network and described how it produces signals. We have also stressed that the dynamics of the network is determined by a dynamical law that requires that both input and output signals in the network respect the underlying mathematical Riemann Surface structure of the network under distortions or deformations. Our next step is to introduce the algebraic function used to describe our special surface network, the Riemann Theta ($\theta$) Function, and the Fey Trisecant Identity it must satisfy if it is to describe a Riemann Surface[12]. With these technical details in place, we then can proceed to study the node events.

## Materials and Methods

### RIEMANN THETA FUNCTION

We have already described how $\sum_g$ is defined in terms of 2*g* topological coordinate loops $(a_i, b_i), i = 1, 2, \cdots g$ ; and *g* one-forms $\omega_i(u)du$. From them we first generate a set of algebraic variables $(n_i, z_i, \Omega_{ij})$ that capture geometric and smoothness features of the Riemann Surface and then use them to define the Riemann Theta Function. These variables were already described in an intuitive way, now we give the formal definitions and explain that they have geometric and topological meaning.

We start by normalizing one-forms so that an integral once round $a_i$ loop is, either plus or minus,

$$\int_{a_i} \omega_i(u)\, du = \pm 1$$

The result represents a topological winding number associated with the loop $a_i$. The two signs correspond to the two possible ways winding can happen; clockwise or anticlockwise. Thus, associated with a loop $a_i$ one can associate a winding $n_i$, which can take any possible integer value.

Next, for any given point $z$ of $\sum_g$ it is possible to generate *g* complex numbers by

$$z_i = \int_{z_0}^{z} \omega_i(u)\, du$$

with $i = 1, 2, \cdots g$, where $z_0$ is an arbitrary fixed point on $\sum_g$ . Thus, a single variable point on the Riemann surface generates a set of *g* variable points that come from the presence of the *g* smooth one-forms of the Riemann Surface. This is a natural way of feeding in smoothness in an algebraic way. Next, a complex matrix can be constructed by integrating one-forms, but this time over the $b_i$ loops

$$\Omega_{ij} = \int_{b_i} \omega_j(u)\, du$$

with $i, j = 1, 2, \cdots g$. This matrix has been proved to be symmetric and its imaginary part positive[10]. It describes the complex connectivity of the Riemann surface.

Finally, an additional set of variables $(\alpha_i, \beta_i)$ that can only take the values 0 or 1/2 can be introduced. These discrete variables are called characteristics and represent the spin structure of $\sum_g$ in an algebraic way in the Riemann Theta Function. The characteristics allow that fractional winding numbers when one-forms that are integrated around the $a_i, b_i$ loops, are possible[8,9].

These characteristics can also be used to define topological number *W*.

$$W = 4\sum_{i=1}^{g} \alpha_i \beta_i$$

With all variables required defined, we can now define the theta function with characteristics[10]:

$$\theta_{[\alpha_i,\beta_i]}(\Omega, z_i) = \sum_{n_1,..n_g=-\infty}^{+\infty} e^{\sum_{a,b} \pi i (n_a+\alpha_a)\Omega_{ab}(n_b+\alpha_b)+2\pi i (z_a+\beta_a)(n_b+\alpha_b)\delta_{a,b}}$$

where $\delta_{a,b}$ is the Kronecker delta function.

The Riemann Theta Function depends on *g* complex numbers $z_i$

$$z_i = \int_{z_0}^{z} \omega_i$$

generated from two points $(z_0, z)$ on $\sum_g$ . Thus, the Theta Function is defined on a *g* dimensional space of complex numbers and has periodicity properties, inherited from the periodicity of the integrals of $\omega$ over the closed loops $(a_i, b_i)$ of $\sum_g$ . This complex space with the periodicity features factored out is the *g* dimensional space called the Jacobian, $J(\sum_g)$[10]. Points on $\sum_g$ on the other hand, are described by just a single complex variable. To understand how the Theta Function, defined on a space of *g* complex dimensions can represent $\sum_g$ , a function of just one complex variable, we make use of the Jacobi Inversion Theorem[13] which is stated (App. V). The basic idea is that for *g* points on $J(\sum_g)$ there are *g* related points on $\sum_g$ .

## LOCAL DISTORTION WITHIN THE THETA FUNCTION

We now define local pinch deformations. In the pinch limit, the radius of a tube loop at a point on a surface is reduced to zero thus moving this point to the center point of the tube, which is a real number. This geometric pinch deformation process can be described in terms of an integral of one-forms along the tube loop. The set of one-forms close to the center point of the tube can be expanded as a Taylor expansion about the center point so that, intuitively, the distortion parameters correspond to the Taylor expansion's coefficients. Since there are *g* one-forms at a point on the surface, each distortion term will have *g* distortion parameters. To get a variety of response solutions it turns out to be necessary to expand the one-forms keeping only the first and third derivative terms[14]. Thus, the variables of the Theta Function collapse to a pair of real numbers that can be interpreted as (*x*, *t*) that are multiplied by factors $W_i, V_i, \quad i = 1, 2, \cdot\cdot\, g$ that represent the nature of the pinch deformation (App. II B). Since under a pinch deformation the circumference of a tube at the pinch point goes to zero and all *g* complex variables of $J(\sum_g)$ collapse to multiples of a single point of $\sum_g$ where the multiplying factors are the distortion input signal specific parameters. Thus, in the pinch limit the Riemann Theta Function now becomes a function on $\sum_g$ .We make these remarks clear by the following sketch where the technical details are omitted.

A pinch deformation at a point $z$ on $\sum_g$ has an effect on the *g* variables $z_i$ of the theta function. These variables are related by the equation

$$z_i = \int_p^z \omega_i(w)\, dw$$

with $z$ and $p$ as points on $\sum_g$ , the latter being the fixed. Consider a circular arc path joining both points (Fig 2A). In the pinch limit, $z$ approaches to $p$, i.e., $z \to p$ as the radius of the circle with center $z = z_0$ inside the tube, so that the arc length connecting both points also becomes very small. Thus, we have

$$z_i \to \int_p^z \omega_i(w)\, dw$$

$$\to (z - p)\omega_i(z_0)$$

when $z$ is close to $p$. As both of these points are close to the center of the tube, $z = 0$ we approximated $\omega_i(w)$ by its value at the center of the tube, namely by $\omega_i(z_0)$. With this done the *g* points of the theta function become

$$z_i \approx \omega_i(z_0)z$$

Thus, in the pinch limit all the variables of the Theta Function are proportional to the point $z$ which is a point on $\sum_g$ close to the center of the tube. We have set $p = 0$. The proportionality factor $\omega_i(z_0)$, defines the nature of the pinch deformation at point $z$. This sketch is only illustrative. The proper technical set up is given elsewhere (App. II B). We conclude this section by making two remarks.

$\sum_g$ and the algebraic Riemann Theta Function can be constructed from a hyperelliptic equation but with spin structure information about $\sum_g$ added in, that is compatible with the hyperelliptic equation[15,16].

The hyperelliptic equation has important features. It allows the maximum possible spin structures on its associated Riemann Surface[16]. It allows the maximum number of subunits connected Riemann Surface[17]. This means it permits a large of specialized functional subunits of the network to exist, and it can generate a vast number of diverse non-linear excitations by pinch deformations on its subunits[11,14].

## Results

We sketched some essential features of pinch deformations. We drew attention to the transient topological changes they initiate and the fact that the response signals generated by such pinch deformations can be shown to carry with them topological information as well as geometric pinch deformation information. With the mathematical representation fully in place we explore once more the node event. Pinching distortions have three effects: they increase local voltage values (since the surface is charged), they reduced the original genus *g*, and if enough pinching deformations are applied reduce the genus *g* of a system and its spin structure topology number *W* to zero value, and by these topological global processes produce one-dimensional signals.

The exact nature of response of the surface to such pinch deformations can be found by using the dynamical law for the network. The law states that since the Riemann Theta Function describes a Riemann Surface $\sum_g$ only if it satisfies the non-linear Fay Trisecant Identity[12,14], (App. VI), all responses to deformations must satisfy the pinch deformed form of the identity, which in our case,

gives the result that responses to pinch deformations are Theta Function solutions of a set of non-linear Schrödinger differential equations, where the variables of the Theta Function are distorted by the pinch deformation. This result applies to any subunit $\sum_k$ from $\sum_g$ ($k < g$) that is pinched. Thus, responses to pinch deformations in a subunit, produce responses that are Riemann Theta Functions with their variables distorted by the pinch deformations, which travel to other subunits of the network. In particular the response of a subunit of genus *k*, to *k* pinch deformations that reduces its genus to zero, are a train of *k* one-dimensional solitons, each of which carries the spin structure topological charge *W* as well as geometric pinch deformation information.

There is a variety of soliton solutions of the non-linear Schrödinger equation. Here we look at bright-soliton and dark-soliton solutions (Fig 3). They behave as propagating one dimensional pulse excitations through the surface of $\sum_g$ . Non-propagating local transient solutions of the non-linear Schrödinger equation are also possible.

The one dimensionality of the solution comes from the fact that a pinch deformation forces surface points to the center of the tube pinched (Fig 2). The solutions do not describe the motion of the pinch point, but have a voltage profile determined by the nature of the local distortion and the global properties of the $\sum_k$ that participates to generate it. The idea is that a subunit $\sum_k$ generates a Riemann Theta Function signal that then propagates to other subunits $\sum_k$ by the interconnected network ($\sum_g$ ). Such a scheme is possible since a Riemann Surface represented by a hyperelliptic equation has a modular structure[17].

## ANALYTIC EXPRESSION FOR MULTI-SOLITON AS VOLTAGE PULSES

The expression of multi-soliton pulses solutions[10], (App. VI and VII), can be numerically evaluated (Fig 3). An example[11] of such solution found is

$$\psi_j(x,t) = A_j \frac{\theta\left(\vec{Z} - \vec{d} + \vec{r}(j)\right)}{\theta\left(\vec{Z} - \vec{d}\right)} e^{-i\left(E_j x - F_j t\right)}$$

where

$$r(j) = \int_{a_{(k+1)}}^{a_j} \omega_j(z)\, dz$$

$$\vec{Z} = i\vec{V}_{a_{k+1}} x + i\vec{W}_{a_{k+1}} t$$

$$K_1(a,b) = \frac{1}{2}\frac{\Delta_a \theta[\delta](0)}{D_a \theta[\delta](0)} + D_a \ln\theta\,[\delta]\left(\int_a^b\right)$$

$$K_2(a,b) = -\Delta_a \ln\theta\left(\int_a^b\right) - D - a\ln\left(\theta\left(\int_a^b\right)\theta(0)\right) - \left(D_a \ln\theta\left(\int_a^b\right) - K_1(a,b)\right)^2$$

$$E_j = K_1\left(a_{k+1}, a_j\right)$$

$$F_j = K_2\left(a_{k+1}, a_j\right) - 2\sum_{i=1}^{k} q_1(a_{k+1}, a_i)$$

$$q_1(a,b) = D_a D_b \ln\theta\,[\delta]\left(\int_a^b\right)$$

$$q_2(a,b) = \frac{D_a\theta[\delta](0)D_b\theta[\delta](0)}{\theta[\delta]\left(\int_a^b\right)^2}$$

and $\vec{d}, A_j$ are constants. Each pulse soliton contains the same pinch deformation parameters through the variable $\vec{Z}$ [11]. Solutions without oscillation factors have also been found[18].

It should be noted that *k* pinches are involved in the solution $\psi_j(x,t)$. Thus, a large multi-soliton response is generated by contributions from a large number of pinch deformations.

Soliton solutions can be physically interpreted as voltage variations (App. IV B).

Numerical evaluations of multi-soliton solutions belonging to two different classes, bright and dark solitons are here determined. We consider four examples.

We illustrate the approach by numerically evaluating $\psi_j^2$ for four multi-solitons. Here we find first the dark solution for *k* = 3 and *k* = 2, and then invert them to obtain the bright soliton solutions (Fig 3). The soliton nature of both solutions is shown numerically.

In the numerical evaluations of the three and two pulses multi-soliton for dark and bright solutions are considered. It is found that not all input signal parameters lead to excitations. The solution's pinch deformation parameters fix the rate at which the soliton pulses appear, as well as the gaps between them through the parameters $\vec{Z}$ and $\vec{r_j}$ of the solutions where the parameters $T_{j,\beta}$ fixes the shape of those pulses.

We write

$$V = (a_k, b_k) = a_k + ib_k$$

$$W = (c, d) = c + id$$

$$i = +\sqrt{-1}, k$$

$$(V_k, W_k) = (a_k, b_k, c_k, d_k)$$

$$k = 1, 2, 3$$

The pinching loops for the $k = 3$, dark solutions are real points ($a_1 = -3.999, a_2 = -3.95, a_3 = -3.92, a_4 = -3.91$), they are zeros of the hyperelliptic equation. The Riemann Surface is constructed using this information and choosing branch point locations in the complex plane located to be: (-4, -3, -2, -2 + $\epsilon$, 0, 0, + $\epsilon$, 2, 2 + $\epsilon$), with $\epsilon = 10^{-10}$. The input data is displayed (Table 1).

**Table 1**

| Pinch distortion | Code | Network | T or E |
|---|---|---|---|
| P. d. (1) | (0, -2.5873, 0, 11.5975) | (1, 1, 1) | T |
| P. d. (2) | (0, -309581, 0, 14.706) | (1, 1, 1) | T |
| P. d. (3) | (0, -3.2384, 0, 15.6638) | (1, 1, 1) | T |

For the $k = 2$ case the branch points are (-2, -1, 0 + $\epsilon$, 2 + $\epsilon$), The pinching loops are ($a_1 = -1.9, a_2 = -1.11, a_3 = -1.8$). Input data displayed (Table 2).

**Table 2**

| Pinch distortion | Code | Network | T or E |
|---|---|---|---|
| P. d. (1) | (0, -1.9142, 0, 2.5916) | (1, 1) | T |
| P. d. (2) | (0, -2.2790, 0, 3.6734) | (1, 1) | T |

Solutions of the non-linear Schrödinger equation represent responses to local pinch deformations of the Riemann Surface network studied. The equation has a non-linear term of the form

$$\sum_{i=1}^{k} s_i \psi_i(x,t)^2 \psi_j(x,t), \qquad j = 1,2 \cdot\cdot k$$

where $s_i = \pm 1$, for a soliton $\psi_j(x,t)$. Different choices for the sign factor $s_i$ lead to different types of solutions. For dark solutions $s_i = +1$ for all $k$ values, while for bright solutions $s_i = -1$ for all $k$ values. Other sign selections produce voltage pulse excitations of different shapes and are topologically distinct.

The numerical solution fixed the index $k$ of the solutions displayed to $k = 2$ and $k = 3$ to numerically determine two and three dark soliton solutions. The propagation speed of the solitons and their amplitudes found numerically can be adjusted by a suitable choice of scale parameters (App. IV B). In the case of $k = 2$ there are eight, and for $k = 3$ twelve distortion parameters. These parameters are assembled together by characteristics $\alpha_i$ that identify the section of the network responsible for the local distortion (i.e., excitation). All characteristics are set to be equal to 1/2, this means that in the soliton limit all network paths of the unit producing the signal are used. We note the vector $\vec{Z}$ fixes the rate at which the spikes pulses arrive. The solutions show that gaps between the soliton pulses and their rate of production carry information as they are sensitive to the pinch distortion parameter values used to generate them. The gaps depend on the form of the period matrix in the pinch limit.

The multi-soliton pulses have an information carrying substructure that originates from input distortion signal parameters at multiple pinch locations of the surface of the network. This substructure is carried directly by the solutions and also indirectly in the appropriate connectivity

matrix elements $\Omega_{ij}$ of the network responsible for such signal. The multi-soliton pulses then can transport and carry the pinch distortion details.

**Discussion**

In this paper we introduce a two-dimensional mathematical surface network, which is a special Riemann Surface that can be parametrized by the algebraic hyperelliptic equation, that exactly captures any hypothetical topological connectivity, and includes surface electrons. The dynamical law for this network required that all activities of the network must conform to the mathematical structure of the surface introduced. Thus, both input signals as well as the responses they produce are required to satisfy the mathematical properties of our special Riemann Surface. To study the dynamical behavior of the Riemann Surface under deformations we introduced the Riemann Theta Function. But for this description to be valid, the Theta Function had to satisfy a nonlinear identity called the Fay Trisecant Identity[19]. Under the pinch deformations introduced, the identity becomes a set of nonlinear Schrödinger equations. Hence the dynamical law requirement implies that responses to pinch deformations are Theta functions, with pinch deformed variables, that satisfy the set of nonlinear Schrödinger equations.

We pointed out that pinch deformations, which have signal specific geometric distortion parameters, also change the two topological structures present in the network: one coming from its connectivity and the other from the spin of the surface electrons. The signals then generated carry with them both, the geometric and the topological information respectively.

Using this mathematical scheme, a special surface network can generate a wide variety of one-dimensional voltage pulse signals that carry transient structural information regarding input, topology changing, local pinch deformations. Transient, because it is a traveling signal, and structural because the signal carries within the parameters of the structure that produced it. The network itself is then a special electroconductive continuum, similar to the syncytium proposed by Golgi in his reticulate theory[20]. Recently, such a kind of neural anatomy has been demonstrated in nature with neural nets in ctenophores[21], providing light on the possibility that Ramón y Cajal's neuronal doctrine[22] is not unique as a solution for neural networks.

The perspective developed here may offer a new light to our understanding of information and plasticity in the brain. Commonalities between the network as a mathematical object and a biological brain could be considered. First, the topological connectivity architecture of the network can capture that of any hypothetical brain connectome. The topological method of signal generation that is proposed is robust and can work for a wide variety of geometrically different but topologically equivalent systems. Secondly, if we think of the mathematical surface as one that covers the brain's assembly of individual three-dimensional neurons linked together via synapses, the topological changes required for signal generation can be interpreted as revealing the underlying nodal structure in the system. From this picture we can identify each signal producing neuron as the location where surface coordinates collapse, due to pinch deformations, to produce one-dimensional signals, and such signals can only be generated if the network is a specific surface network with loops and electrons.

On that basis we speculate on the way the mathematical results could correspond to observed brain events. The brain is not structurally a continuum. Neurons form a network by being in contact with each other, but still separated from each other by synaptic clefts. A single reticular like formation could conceptually overlap with a brain's connectome forming a unit. A continuous, virtual surface that roughly would correlate with a cloud of specific ions that surround the neural membrane, could be represented by such a proposed structure. The presence of gap junctions (electric synapses) in nature, aligns with the reticular continuum concept. The interconnectivity captured by the genus *g* and the electric properties by the topological number *W*.

Local depolarization events produced by inward currents as a result of synaptic excitatory stimulation could find a descriptive parallel with the reduction of any $a_i$ cycle in $\sum_g$ , as part of a charged surface they also describe local depolarizations (App. IV A). A full pinch deformation could possibly find correspondence with a full depolarization of a branch or the section of a branch, correlated with punctual increases of intracellular, local ionic concentrations (e.g., $Na^+$, $Ca^{2+}$), produced by inward depolarizing currents. The physicality of excitatory synaptic connections as a possible correlate to pinching (local distortion that generates an increase in depolarization) makes it a topologically stable event, fixed in the geometry of the full network. It would be stable within the coordinate system that describes it, which in biology would also get strengthened through potentiation[23,24].

Solitons as traveling non dissipative signals could correlate with action potential trains in the nervous system. Solitons $\psi(x,t)$, as electromechanical pulses (App. IV B) would be observed in the electric charge, as well as a "mechanical" pulse in the lattice of the theoretical surface (Fig 3). A similar phenomenon has been observed on axons when firing action potentials[25]. Interestingly the structure here proposed predicts that such traveling electric signals, if strong or repetitive enough, and because they are one-dimensional current pulses traveling through the center of an electrocharged tube, would generate a helical non-transient structure on the surface itself, preserved by the spin structure (App. VIII). Because these helical structures are generated by a signal that is defined by parameters present in the Theta Function, they themselves would also be defined by the same parameters (App. VII and VIII). An engraving event that is generated and corresponds to the same signal that was transmitted, resonates with Richard Semon's concept of memory[26]. These transient signals carry charge and have a shape that is determined by the input signal specific geometric deformations. As they move through the network, they generate a transient magnetic field that acts on surface spins present and aligns them to form topologically stable non-transient helical structures with well-defined excitation frequencies. These topological structures in the pathways of the network also result in a stable non transient magnetic record of the transient signal that created them. Such a structure has been observed to form in solid state physics[27], under similar conditions as the ones described. Under suitable excitations of appropriate frequency (i.e., resonance), the stored magnetic record could be reactivated by such an event (App. VIII B). Then hypothetically, the structural transient information (i.e.: the topological parameters carried by the soliton, a traveling pulse) could then be recorded in a non-transient magnetic structure within the network itself, and by this we mean a magnetic, helical structure on the surface through where the signal passed, made stable and permanent, by the interaction of spins present in the surface electrons that were affected and aligned by the original passing signal (App. VIII A).

There is as yet no evidence of such magnetic helical structures in biology, but the magnetic field of action potentials along the axonal tube has been measured and used to accurately reconstruct the shape of action potentials[28]. A speculation for a cellular rigid structure that can contain a dense array of molecules in tubular rings on which then electrons (spinors) are organized, through which current is passed orthogonally, can find some correspondence with protein rich structures through which action potential travel, such as the axon initial segment[29,30] and the nodes of Ranvier[31]. On regards to how biological systems would behave as surfaces on such conditions, phospholipids bilayers have been observed to responsive and plastic to previous stimulation by exhibiting a long-term potentiation (LTP) type of behavior[32], demonstrating that neuronal membrane can be sensitive at least electrostatically. As well, evidence that electric fields may help organize neural cytoskeleton has been proposed[33].

The approach presented has several features. It is essential that the two topological features described (*g* for the connectivity, *W* for spin structure) are present in order to generate the wide variety of signals we have discussed. The hypothetical concept that surface electrons through the formation of non-transient structures could form record traces of transient signals, is novel and appears as an emergent property from within the framework. Here we offer a perspective which

the existence of spin half particles become essential for a recording event. We are aware that in the process of biological memory creation intricate biochemical processes play essential roles[24], however, the issue of how memories are stored is still under debate[34,35,36]. Recent studies have shown that memory can persist in the structure of the neural circuit despite the loss of recall in cases of amnesia[37,38]. This scheme presents a new possibility for memory, one that incorporates topological location, connectivity, and signals, while offering a unifying consistency.

We attempted to globally define an electro-conductive network where a coherent link could be made between signal emission and local input. We believe that the findings presented could offer a new point of view to analyze and understand a network that possesses a self-interpretating coding system, since the approach can relate the functioning a brain to its form at the most fundamental level of signal generation. Recent work supports[39] such a holistic viewpoint of brain function from a different perspective. It is shown by detailed analysis, that observed patterns of brain activities can be best represented by using hypothetical global waves that are dependent on the measured geometric properties of the biological brain, and then showing that these waves can be used to fit regions of brain activity very well, thus relating brain function displayed by brain activity regions, to its form as described by the brain's measured surface geometry.

In summary we introduce a special surface network with electric charge that could be used to capture the topological connectivity of any possible brain connectome and illustrated that a variety of one-dimensional signals can be generated within the system, by topological deformation of subunits. This model was obtained by using a general dynamical law of compatibility.

Topology has grown in importance as a way to explore the brain and its global features for instance to understand connectivity data or for analyzing algebraic structures associated with signals[40,41,42,43,44], but we believe that that linking signal generation to topological structural plasticity provides a novel way of using topology to store latent information in the brain.

**Acknowledgements**

The authors would like to thank Mike Coey, Kumar Gupta, Mani Ramaswami, and Arnab Das for encouragement, Paul Voorheis for reading through an earlier version of the manuscript and making helpful editorial suggestions, Raul Ramos for his help with the figures, Christian Klein and Jörg Frauendiener for their kind assistance and for supplying codes used in their work on Riemann surfaces, and also to Mauro Ferreira for his guidance and support.

**Author Contributions**

S.S. performed all mathematical procedures. D.M. performed the MATLAB calculations and experiments. S.S. and M.P. wrote the manuscript draft. S.S., T.R., and M.P. guided, discussed, analyzed and formulated the ideas and developed the manuscript structure. S.S., T.R., and M.P. edited the manuscript. All authors approved of the submitted manuscript.

**References**


1. Arendt, D., Tosches, M.A., and Marlow, H., From nerve net to nerve ring, nerve cord and brain - evolution of the nervous system. *Nature Reviews Neuroscience* 17: 61-72 (2016)
2. Liebeskind, B.J., Hillis, D.M., Zakon, H.H., and Hofmann, H.A., Complex homology and the evolution of nervous systems. *Trends in Ecology and Evolution* 31(2): 127-135 (2016)
3. Roberts, R.J.V., Pop, S., Prieto-Godino, L.L., Evolution of central circuits: state of the art and perspectives. *Nature Reviews Neuroscience* 23: 725-743 (2022)
4. Nash, C. and Sen, S., “Topology and Geometry for Physicists.” (Academic Press 1988)
5. Teleman, C., ”Riemann Surfaces. Lent Lectures.” (Berkeley Math 2003)
6. Munkres, J., “Topology. Pearson New International Edition.” (Pearson 2014)
7. Bak, J. and Newman, D.J., “Complex Analysis.” (Springer 2010)
8. Atiyah, M. F., Riemann surfaces and spin structures. *Annales Scientifique de l’École Normale Supérieure, quatrième série*, 4: 47-62 (1971)
9. Mumford, D., Theta characteristics of an algebraic curve. *Annales Scientifique de l’École Normale Supérieure, quatrième série,* 4: 181-192 (1971)
10. Mumford, D., “Tata Lectures on Theta II.” (Brikhäuser 1984)
11. Kalla, C., New degeneration of Fay’s identity and its application to integrable systems. *International Mathematics Research Notices* 2013: 4170-4222 (2012)
12. Sen, S. and Raina, A.K., Grassmannians, multiplicative ward identities and theta-function identities. *Physics Letters B* 203: 256-262 (1988)
13. Guardia, J., Jacobian nullwerte and algebraic equations. *Journal of Algebra* 253: 112-132 (2002)
14. Arbarello, E., Sketches of KdV. *Contemporary Mathematics* 312: 9-69 (2002)
15. Kallel, S. and Sjerve, D., Invariant spin structure on Riemann surfaces. *Annales de la Faculté des Sciences de Toulouse Mathématiques* 19: 457-477 (2010)
16. Krazer A., “Lehrbuch der Thetafunktionen.” (Leipzig B.G. Teubner 1903)
17. Harnack, A., Ueber die Vieltheiligkeit der ebenen algebraischen Curven. *Mathematische Annalen* 10: 189-198 (1876)
18. Previato, E., Hyperelliptic quasi-periodic and soliton solutions of the nonlinear Schrödinger equation. *Duke Math Journal* 52(2): 329-377 (1985)
19. Fay, J.D., “Theta functions on Riemann Surfaces.” Lecture Notes in Mathematic 352. (Springer-Nature 1973)
20. Golgi, C., “Sulla Fina Anatomía degli Organi Centrali del Sistema Nervoso.” (Stefano Calderini e Compagno 1885)

21. Burkhardt, P., Colgren, J., Medhus, A., Digel, L., Naumann, B., Soto-Angel, J.J., Nordmann, E.L., Sachkova, M.Y., and Kittelmann, M., Syncytial nerve net in a ctenophore adds insights on the evolution of nervous systems. *Science* 380: 293-297 (2023)

22. Ramón y Cajal, S., Estructura de los centros nerviosos de las aves. *Revista Trimestral de Histología Nórmal y Patológica* 1:1-10 (1888)

23. Asok, A., Leroy, F., Rayman, J.B., and Kandel, E.R., Molecular mechanisms of the memory trace. *Trends in Neurosciences* 42: 14-22 (2019)

24. Lynch, M.A., Long-term potentiation and memory. *Physiological Reviews* 84: 87-136 (2004)

25. El Hady, A. and Machta, B., Mechanical surface waves accompany action potential propagation. *Nature Communications* 6: 6697 (2015)

26. Semon, R.; "Die Mneme als erhaltendes Prizip im Wechsel des organischen Geschehens." (Wilhelm Engelmann 1904)

27. Uchida, M., Onose, Y., Matsui, Y., and Tokura, Y., Real-space observation of helical spin order. *Science* 311: 359-361 (2006)

28. Barry, J., Turner, M.J., Schloss, J.M., Glenn, D.R., Song, Y., Lukin M.D., Park, H., and Walsworth, R. L.; Optical magnetic detection of single-neuron action potentials using quantum defects in diamond. *Proceedings of the National Academy of Sciences*, 113: 14133-14138 (2016)

29. Hamdan, H., Lim, B.C., Torii, T., Joshi, A. Konning, M., Smith, C., Palmer, D.J., Ng, P., Leterrier, C., Oses-Prieto, J.A., Burlingame, A.L., and Rasband, M.N., Mapping axon initial segment structure and function by multiplexed proximity biotinylation. *Nature Communications* 11: 100 (2020)

30. Leterrier, C., The axon initial segment: an updated viewpoint. *The Journal of Neuroscience* 38(9): 2135-2145 (2018)

31. Rasband, M.N. and Peles, E., The nodes of Ranvier: molecular assembly and maintenance. *Cold Spring Harbor Perspectives in Biology* 8(3): a020495 (2016)

32. Scott, H.L., Bolmatov, D., Podar, P.T., Liu, Z., Kinnun, J.J., Doughty, B., Lydic, R., Sacci, R.L., Collier, C.P., and Katsaras, J., Evidence for long-term potentiation in phospholipid membranes. *Proceedings of the National Academy of Sciences USA* 119(5): e2212195119 (2022)

33. Pinotsis, D.A., Fridman, G., and Miller, E.K., Cytoelectric coupling: Electric fields sculpt neural activity and "tune" the brain's infrastructure. *Progress in Neurobiology* 226: 102465 (2023)

34. Ortega-de San Luis, C. and Ryan, T.J.; Understanding the physical basis of memory: Molecular mechanisms of the engram. *Journal of Biological Chemistry* 298(5): 101866 (2022)

35. Poo, M.M., Pignatelli, M., Ryan, T.J., Tonegawa, S., Bonhoeffer, T., Martin, K.C., Rudenko, A., Tsai, L.H., Tsien, R.W., Fishell, G., Mullins, C., Gonçalves, T.J., Shtrahman, M., Johnston, S.T., Gage, F.H., Dan, Y., Long, J., and Buzsáki, G., What is memory? The present state of the engram. *BMC Biology* 14(40): 1-18 (2016)

36. Tonegawa, S., Pignatelli, M., Roy, D.S., and Ryan, T.J., Memory engram storage and retrieval. *Current Opinion in Neurobiology* 35: 101-109 (2015)

37. Guskjolen, A., Kenney, J.W., de la Parra, J., Yeung, B.R.A., Josselyn, S.A., and Frankland, P.W., Recovery of “lost” infant memories in mice. *Current Biology* 28: 2283-2290 (2018)

38. Ryan, T.J., Roy, D.S., Pignatelli, M., Arons, A., and Tonegawa, S., Engram cells retain memory under retrograde amnesia. *Science* 348: 1007-1013 (2015)

39. Pang, J.C., Aquino, K.M., Oldehinkel, M., Robinson, P.A., Fulcher, B.D., Breakspear, M, and Fornito, A., Geometric constrains no human brain function. *Nature* (2023).

40. Blevins, A.S. and Bassett D.S., Topology in biology. *Handbook of the Mathematics of Arts and Sciences*: 1-23 (2020)

41. Curto, C., What can topology tell us about the neural code? *Bulletin of the AMS* 54: 63-78 (2017)

42. Kanari, L., Dlokto, P., Scolamiero, M., Levi, R., Shillcock, J., Hess, K., and Markram, H.; A topological representation of branching neuronal morphologies. *Neuroinformatics* 16: 3-13 (2018)

43. Marcolli, M., Gamma spaces and information. *Journal of Geometry and Physics* 140: 26-55 (2019)

44. Reimann, M.W., Nolte, M., Scolamiero, M., Turner, K., Perin, R., Chindemi, G., Dlotko, P., Levi, R., Hess, K., and Mrakram, H., Cliques of neurons bound into cavities provide a missing link between structure and function. *Frontiers in Computational Neuroscience* 11: 48 (2017)

**Figures and Tables**

**Figure 1.**

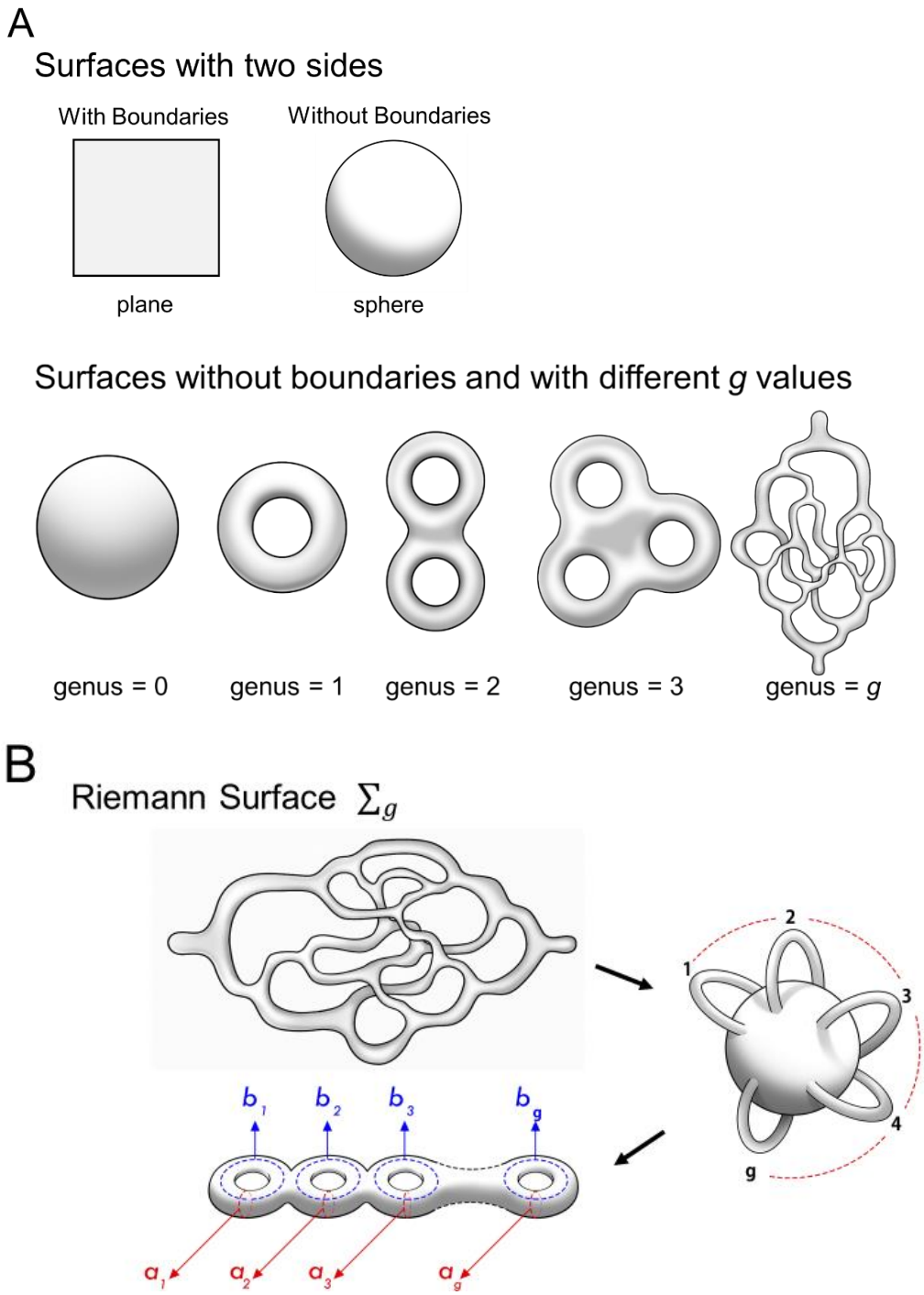


**Figure 1:** Topology studies surfaces in a holistic way. In this discipline, objects that can be transformed into each other are regarded as the same. **A.** A surface with two sides can have a boundary or not have a boundary. **B.** A surface without boundary, in topology, is equivalent to a sphere with g handles or an array of g donuts. The number g is the genus of the surface. All objects of genus g are the same. So that a sphere, a

cube, or a tetrahedron are the same in topology ($g$ = 0), a donut and a teacup can be regarded as the same ($g$ = 1), but not to a teapot ($g$ = 2) nor to a pretzel ($g$ = 3)**.** Our surface has fixed but unknown genus g.

**Figure 2.**

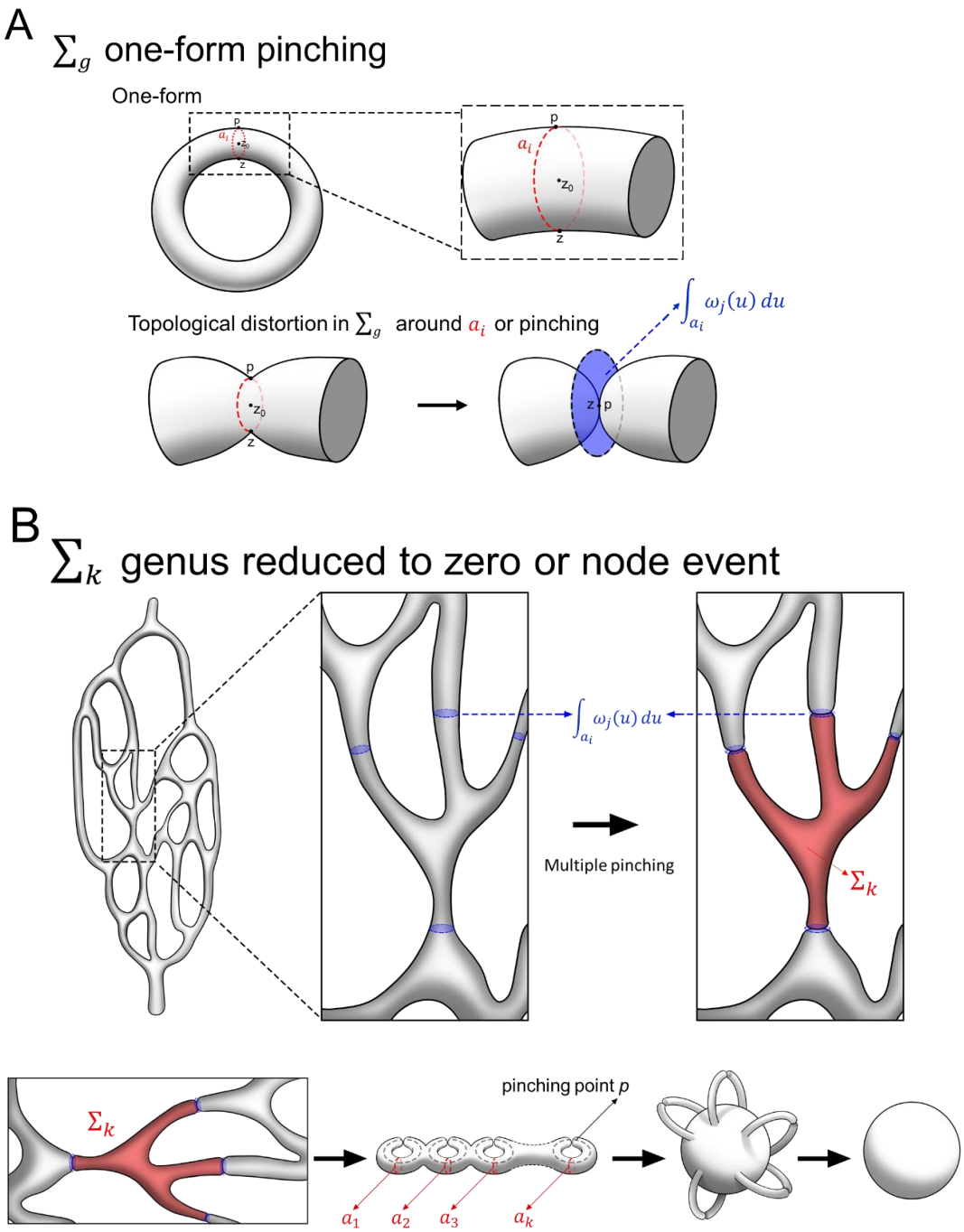


**Figure 2:** Local topological pinch deformations reduce, at a defined point, the circumference of a loop round a one-form $\omega_j(u)$ to zero. **A.** The dynamic law proposed is implemented by taking the limit of the two surface-points ***p*** and ***z*** approaching each other so that an arc joining them, a sub-section of an $a_i$ loop connects them approaches zero. In this way the pinch deformation respects the Riemann Surface structure. This limit can be studied by considering the integral $\int_{a_i} \omega_j(u)\, du$ (see text for details). **B.** By pinching *k* one-forms that belong to $\Sigma_k$, which is a sub-unit of the full surface-network $\Sigma_g$, the subunit has its total genus value reduced to zero which transforms it transiently, into a topological sphere. We define this as a node event.

**Figure 3.**

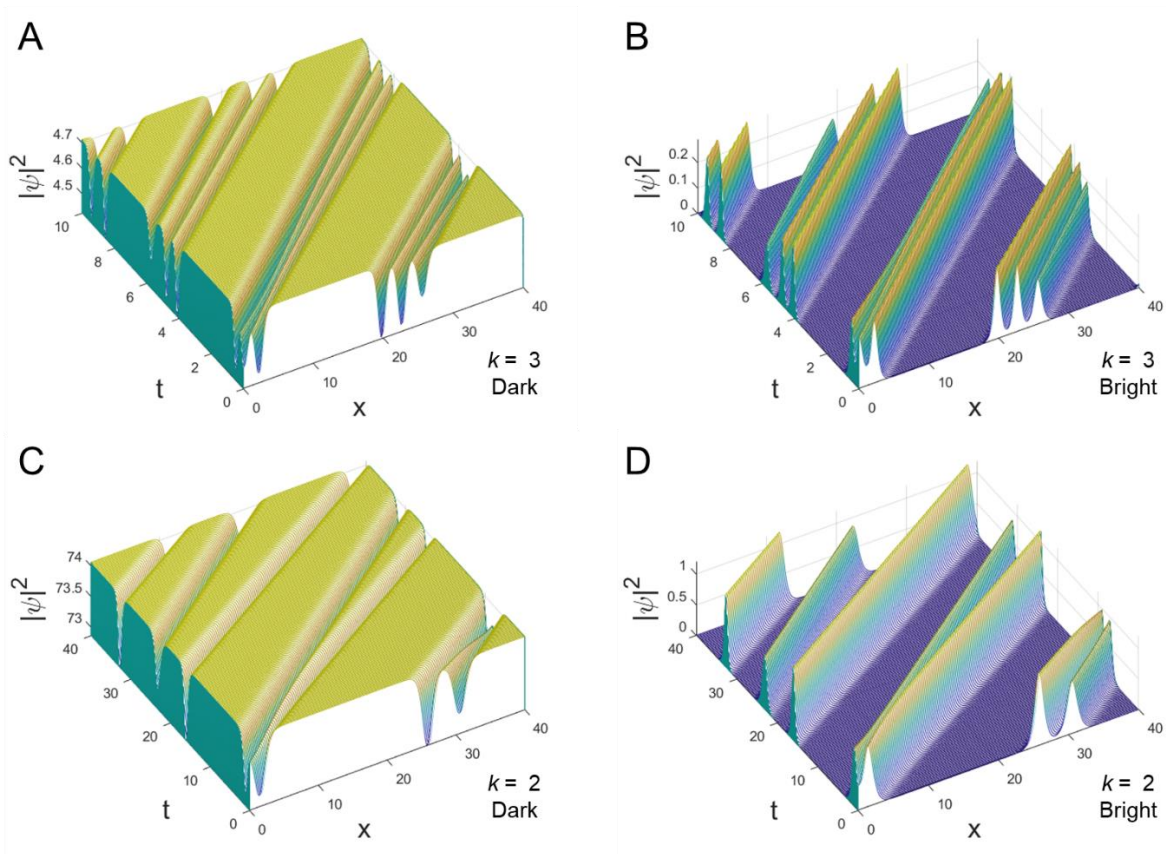


**Figure 3:** Numerical evaluations of multi-soliton solutions $\psi_j(x,t)$ belonging to two different classes, bright and dark solitons are here plotted. The soliton solutions are evaluated as $\psi_j^2$ (MATLAB, MathWorks). For the parameters presented in table 1 for $k = 3$, **A.** One of the solutions defined as dark. **B**. The complementary solution for the same case defined as bright. For the parameters presented in table 2, for $k = 2$, **C.** the dark solution and the **D.** bright solution for the complementary soliton. Dark soliton solutions were obtained first. Bright soliton solutions obtained by inverting the dark solution.

**Table 1.**

| Pinch distortion | Code | Network | T or E |
|---|---|---|---|
| P. d. (1) | (0, -2.5873, 0, 11.5975) | (1, 1, 1) | T |
| P. d. (2) | (0, -309581, 0, 14.706) | (1, 1, 1) | T |
| P. d. (3) | (0, -3.2384, 0, 15.6638) | (1, 1, 1) | T |

**Table 2.**

| Pinch distortion | Code | Network | T or E |
|---|---|---|---|
| P. d. (1) | (0, -1.9142, 0, 2.5916) | (1, 1) | T |
| P. d. (2) | (0, -2.2790, 0, 3.6734) | (1, 1) | T |

**Supporting Information Text**

Appendix

**I.** Riemann Surface

A mathematical result tells us[1] that all Riemann Surfaces can be viewed as geometrical representations of polynomial equations of two complex variables, $P(z,w) = 0$, where,

$$P(z,w) = a_0(z) + \cdots a_i(z)w^i + \cdots a_m(z)w^m = 0$$

and the coefficients $a_i(z)$ are polynomial functions of $z$. The degree *n* of the polynomial, which means the highest power of $n = l + k$ of terms $z^k w^l$ present in $P(z,w)$ fixes the genus *g* of the surface to be

$$g = \frac{(n-1)(n-2)}{2} - N_s$$

where $N_s$ is the number of singular points of the polynomial equation, that is points where;

$$\frac{\partial P(z,w)}{\partial z} = 0$$

Thus, a Riemann Surface is a geometrical representation of a polynomial equation of two complex variables with its genus fixed by the nature of the polynomial. This representation defines the notion of smoothness of the surface. The smoothness of a surface means that the defining polynomial equation can be differentiated an arbitrary number of times. The applying of the classifying surfaces theorem[2], tells us that the Riemann surface of genus *g* can be represented as a connected surface of *g* donuts (tori). Using this representation, the connectivity properties of $\sum_g$ can be described by topological coordinates that are a set of 2*g* closed loops $(a_1, a_2 \cdots a_g;\ b_1, b_2 \cdots b_g)$ (Fig 1B). A particular choice of loops is called marking. The loops chosen are orthogonal which means that two loops from set A $(a_1, a_2, \cdots a_g)$ or set B $(b_1, b_2, \cdots b_g)$ in general do not intersect but a loop $a_j$ from A intersects with loop $b_j$ form B once.

We write these geometric properties as

$$(a_i, a_j) = (b_i, b_j) = 0$$

$$(a_i, b_j) = \delta_{i,j}$$

where $\delta_{i,j} = 1$, when $i = j$ and is zero when $i \neq j$.

There is an additional set of 2*g* discrete parameters called characteristics[3], that can only take the values 0 or ½, and are associated with each loop of the sets A, B. The characteristics describe the spin structure of a Riemann surface.

**II.A** One-forms

The smoothness properties of a Riemann Surface $\sum_g$ , with surface points represented by a complex number $u$, are represented by a set of *g* linearly independent holomorphic differential one-forms $\omega_i(u)du$, $i = 1, 2, \cdots g$ on $\sum_g$ [3].

It has been shown that on a Riemann Surface exactly *g* linearly independent holomorphic one-forms exist. This means that any holomorphic on $\sum_g$ can be written as a linear combination of them with constant coefficients.

A one-form is an object that can be integrated.

Thus, if we write an integral

$$\int f(u)du$$

then,

$$f(u)du$$

is a one-form.

**II.B** Pinched one-forms

We define mathematically a local distortion or pinch deformation. We use the one-forms $\omega_j(u)$ on a Riemann Surface of genus *g* that represents a real hyperelliptic equation. We showed that they are given by

$$\omega_j(u) = \frac{z^{j-1}du}{\sqrt{P(u)}}$$

where

$$P(u) = \prod_{i=1}^{(2g+2)} (u - a_i)$$

Thus, these one-forms depend on the $(2g + 2)$ roots of $P(u)$. We also saw that the $a_i$ cycles of $\sum_g$ have circumferences related to the difference between adjacent roots, $(a_{i+1} - a_i)$ of $P(z)$. Hence a pinch corresponds to two roots of the hyperelliptic equation approaching one another, since when this happens the circumference of the corresponding loop $a_i \to 0$. The pinch point is taken to be inside the interval. There are *g* cycles that can be pinched.

There are *g* functions $\omega_j(u)du$ whose variables can be deformed differently at a given surface point *p*. This point *p* has two coordinates $p_a$, $a = 1, 2$ so that we can write a local distortion as

$$\omega_j\left(p_a + \delta_{a,j}(p)\right)$$

We then can write

$$p = F\left(z_1, .. z_g\right) = F(\vec{z})$$

as a function of *g* variables of $J(\sum_g)$. This is an inverse of the map $p \to (z_1, .. z_g)$. This function is not known. Putting all these pieces together we can write the pinch deformed one-form $\omega_j(p)$, near the pinch point *p* as,

$$\omega_j(p) = \left( V_{a,j}(p) + W_{a,j}(p) k_a(p) + U_{a,j} \frac{k_a(p)^2}{2} + .. \right) dk_a(p)$$

$$D_a F(\vec{z}) = \sum_{j=1}^{g} \partial z_j F(\vec{z})\, V_{a,j}$$

$$\Delta_a F(\vec{z}) = \sum_{j=1}^{g} \partial z_j F(\vec{z})\, W_{a,j}$$

The set of points $j = 1, 2, .. g$ represent pinch locations while $k_a(p),\ a = 1, 2$ can be identified with a point on $\sum_g$ . While the functions $V_{a,j}(p), W_{a,j}(p)$ are the signal specific pinch distortion functions on $\sum_g$ that represent the distortion of the signal generated.

This procedure of deformation described when imposed on the nonlinear Fay Trisecant Identity, turn the identity into a set of nonlinear differential equations known as the nonlinear Schrödinger equation (NLS). The Riemann Theta Function with pinch deformed variables must now be solutions of the NLS in order for it to continue to represent the Riemann Surface. These are soliton solutions[4].

**III.** The hyperelliptic equation $P(u)$ description of a Riemann Surface $\sum_g$

The hyperelliptic equation is given by,

$$y^2 = P(u)$$

Which can be written as,

$$y = \pm\sqrt{P(u)}$$

Near a zero point $x_a$ of $P(u)$ the function becomes

$$P(u) = (u - x_a)K$$

when all the zeros are distinct. Setting

$$w = (u - x_a)$$

we have

$$P(w) = wK$$

Thus, a circle round $w = 0$ changes the sign of $y$ due to the fact that a square root function changes sign under a full circular rotation. Thus, such a function It is not well defined. It's value at a point depends on its history. This problem is overcome by introducing a branch cut, a line, that starts at the point $w = 0$, and the rule that when circling round the point $w = 0$ this line cannot be crossed but the variable moves on to another copy of the complex plane. By this means the function $y$ can be made a well-defined function of the variable $z$ near all its zeros. Thus, the zeros of $P(u)$ determine[5] the branch point locations of $y$ that defines the cuts necessary to make $y(u)$ well defined. These cuts define the topological coordinates of the Riemann Surface associated with the hyperelliptic equation, namely its homology cycles, $a_i, b_i,\ i = 1,2,..g$ as suitable circuits round the branch points. In particular the $a_i$ cycles, that represent loops round the circumference of tubes of $\sum_g$ , are constructed as circuits round a pair of neighboring zeros of $P(u)$ linked together by a branch cut. We next write down the rule for constructing *g* smooth one-forms from $P(u)$. We have

$$\omega_i(u)du = \frac{u^{i-1}du}{\sqrt{P(u)}}\ ,\ \ i = 1,2,..g$$

Now the complex variable $u$ represents a point on the Riemann Surface of genus *g* constructed. We will replace $u$ by $z$ to represent such points. Thus, we have sketched how the topological cycles $(a_i, b_i)$ and the smooth one-forms $\omega_i$ that define a Riemann Surface can be constructed starting from a hyperelliptic equation.

**IV.A** Voltage variations on $\sum_g$ ; Local distortions

The topological tube or handle has electrical and geometrical properties. As charged per definition, we can consider our surface a dynamic dipole layer. The voltage difference of the dipole is then defined as $V_0$.

We want to estimate the equilibrium value between strips of the surface separated by the diameter *r* of the surface tube. The calculation uses the electrical properties and the dynamic laws of quantum electrodynamics. It has been shown[6] using quantum electrodynamics that there is an attractive Casimir-Poldar potential $V_{CP}(r)$, between charged dynamic dipoles layers separated by a distance *r*. The attractive potential is balanced by the elastic properties of the tube and the space contained by it.

We have then

$$V_{CP}(r) = -\frac{V_0}{r^7}$$

which is an attractive potential energy between dynamic neutral particles. It can be understood as a resting potential. Variations of *r*, are then result in voltage changes that reflect changes in the resting potential value.

**IV.B** Voltage variations on $\sum_g$ ; Soliton solutions

All the variables, functions and equations used are dimensionless. This allows flexibility on the nature of the system described. Then, multi-soliton solutions may be interpreted as voltage pulses. Consider the following non-linear Schrödinger equation with dimensional parameters,

$$i\frac{\partial}{\partial t}\psi = -D\nabla^2\psi + g\psi^2\psi$$

where $t$ is time units, $x$ is in length units, $D$ is a dimensional diffusion constant, $\psi$ is in volts and $g$ is a dimensional constant which is a measure of non-linearity. We can rewrite this equation using dimensionless variables, we have

$$t \to \tau = \frac{t}{t_0}$$

$$x \to \frac{x}{x_0}$$

$$D \to D_0 = \frac{x_0^2 D}{t_0}$$

$$g \to g_0 = \frac{g V_0^2}{t_0}$$

Then once units for $t_0, x_0, V_0$ have been chosen, the response solutions generated will represent one-dimensional non-dissipative voltage pulses, and the pinch deformations can be understood as input signals as they induce local voltage changes.

## V. The Jacobi Inversion Theorem

The equivalence of $\sum_g$ and $J(\sum_g)$ is at the level of certain abelian groups called divisors. For $\sum_g$ a divisor *D* is the formal sum of selected points on $\sum_g$ multiplied by integers. These groups establish a relationship between the number of zeros on $\sum_g$ to the corresponding number of zeros of the Riemann Theta Function on $J(\sum_g)$. We have

$$D = \sum_p n_p p$$

The degree of a divisor is defined as

$$degD = \sum_p n_p p$$

For a meromorphic function $f : \sum_g \to C$, a natural notion of a divisor $(f)$ can be introduced. We write

$$(f) = \sum_p \left(ord_p(f)\right)_p$$

This is an enrichment of $\sum_g$ as further structures namely special types of functions are introduced on it. A meromorphic function has simple zeros and poles. The order at a simple pole is minus one, while at simple zero it is plus one. A general result is that the sum of the orders of zeros and poles of a meromorphic function on $\sum_g$ is zero. This translates to the statement that $deg(f) = 0$. We next introduce the Abel-Jacobi map, that maps point $p$ on $\sum_g$ to points on $J(\sum_g)$. We must remember that a point in $J(\sum_g)$ is defined by *g* complex numbers. We have,

$$\mu: \Sigma_g \to J(\Sigma_g)$$

$$\mu = \left(\int_{p_0}^{p} w_i \, , i = 1, 2, \cdots g\right)$$

The point $p_0$ is a fixed reference point on $\sum_g$ with respect to which other points are linked by a path. It is possible to show that the linking path chosen does not matter. The map is then well defined.

This map extends to divisors. For point $p$ in $\sum_g$ we have,

$$\mu\left(\sum_p n_p p\right) = \sum_p \mu(p)$$

We can now state the Jacobi Inversion Theorem: For every point in $J(\sum_g)$ is the image under $\mu$ of a degree zero divisor of the form

$$D = \sum_{i=1}^{g} (p_i - p_0)$$

on $\sum_g$ .

## VI. The Degenerate Fay Trisecant Identity

The one-dimensional solutions were found by exploiting a link between the Riemann Surface and the Riemann Theta Function provided by the Fay Trisecant Identity. In the logic chart (Fig S1) these links are shown. There the identity is also displayed using a different notation[8]. For the sake of completeness, we write down the pinch degenerate limit of this identity based on previous work[4], which takes the form of a nonlinear differential equation. The NLS equations we use, can be derived from this equation.

The functions needed to express the degenerate form of the Fay Trisecant Identity are here defined. Let $a, b$ be distinct points on $\sum_g$ . Fix local parameters $k_a, k_b$in the neighborhood of these points. Let $\delta = (\alpha_i, \beta_i),\ i = 1,2 \cdots g$ be a non-singular odd characteristic. Then for any $\vec{z} = (z_1, \cdots z_g)$, Fay Trisecant Identity is $A = C + D + E$, where

$$A = D_a^2 \left[ \ln \frac{\theta\left(\vec{z} + \int_a^b\right)}{\theta(\vec{z})} \right]$$

$$C = -\left( D_a \left[ \ln \frac{\theta\left(\vec{z} + \int_a^b\right)}{\theta(\vec{z})} \right] - K_1(a,b) \right)^2$$

$$D = -2D_a^2 [\ln \theta(\vec{z})] + K_2(a,b)$$

$$E = -\Delta_a \left[ \ln \frac{\theta\left(\vec{z} + \int_a^b\right)}{\theta(\vec{z})} \right]$$

where $\int_a^b = \int_a^b \vec{\omega}$ and the scalars $K_1(a,b),\ K_2(a,b)$ are given by

$$K_1(a,b) = \frac{\Delta_a \theta[\delta](0)}{2D_a \theta[\delta](0)} + D_a \ln \theta\,[\delta]\left(\int_a^b\right)$$

$$K_2(a,b) = -\Delta_a \ln \theta\left(\int_a^b\right) - D_a^2 \ln\left(\theta\left(\int_a^b\right)\theta(0)\right) - \left(D_a \ln \theta\left(\int_a^b\right) - K_1(a,b)\right)^2$$

where $D_a$ is the operator of directional derivate along the vector $\vec{V} = (V_1, V_2 \cdot\cdot, V_g)$ while $\Delta_a$ is the operator of the directional derivate along the vector $\vec{W} = (W_1, W_2 \cdot\cdot, W_g)$ where these vectors describe the pinch distortion at a point of $\sum_g$ . Thus, the identity is written down for a specific pinch deformation.

The parameters of the pinch deformation at a point *p* of $\sum_g$ are given by the vectors $(\vec{V}, \vec{W})$, as follows,

$$\omega_j(p) = \left(V_{a,j} + W_{a,j} k_a(p) + U_{a,j} \frac{k_a(p)^2}{2} + \cdot\cdot\right) dk_a(p)$$

$$D_a F(\vec{z}) = \sum_{j=1}^{g} \partial_{z_j} F(\vec{z}) V_{a,j}$$

$$\Delta_a F(\vec{z}) = \sum_{j=1}^{g} \partial_{z_j} F(\vec{z}) W_{a,j}$$

where the set of points $a_j, j = 1, 2, \cdot\cdot (g+1)$ represent pinch locations. They are special points of $\sum_g$ related to the location of the zeros of the hyperelliptic equation. The representation of the one-form

$$\omega_j(p) = \left(V_{a,j} + W_{a,j} k_a(p) + U_{a,j} \frac{k_a(p)^2}{2} + \cdot\cdot\right) dk_a(p)$$

parametrizes the signal specific deformations while the range of the label *j* captures the number of pinch points that contribute to the one-dimensional solution. Using this notation multiple component solutions of the non-linear Schrödinger equation[4] can be written down. The one-dimensional limit of this solution is relevant and is explored next (App. VII).

## VII. Soliton Limit

Soliton solutions emerge in the limit when a genus $k$ surface ($\sum_k$ a subunit of $\sum_g$ ; $k < g$) degenerates into one of genus zero. The technical way of doing this has been discussed elsewhere[4]. As a genus zero surface is conformally equivalent to a Riemann Sphere. There is a map $w(p) = w$ which maps a point $p$ on a genus zero surface to a point $w$ on the Riemann Sphere. In the genus zero limit we have the following result,

$$\Omega_{kk} = \ln \epsilon + O(1)$$

$$\Omega_{ik} = \ln \left[ \frac{(w_i - w_k)(s_i - s_k)}{(w_i - s_k)(s_i - w_k)} \right]$$

The diagonal period matrix elements expression from

$$\Omega_{kk} = \int_{u_i}^{v_i} \Omega_{v_k - u_k} + O(\epsilon)$$

where

$$\Omega_{v_k - u_k} = \left( \frac{1}{w - w_{v_i}} - \frac{1}{w - w_{u_i}} \right)$$

and $u_i, v_i$ are poles that appear when double points that result when the genus $k$ surface degenerates to one of genus zero, are desingularized. The meromorphic differentials that then appear on the topological sphere are entirely defined by their behavior near their singularities. In this pinching limit, meromorphic functions also appear associated with the variables $z_i$ regarded as functions of a point $z$ of the Riemann Surface. The reason for the appearance of singularities can be understood. A pinch deformation corresponds to the shrinking of $a_i$ loops of $\sum_k$ . These loops correspond to circuits round neighboring zeros of the hyperelliptic equation that describe a genus $k$ subunit

$$y^2 = \prod_{i=1}^{(2k+2)} (z - a_i)$$

that define branch points of the equation in the complex plane. Thus, a pinch deformation corresponds to two zeros coming together $(a_i, a_{i+1})$. When this happens the associated one-form

$$\omega_j(z) = \frac{z^j dz}{\sqrt{P(z)}}$$

become singular and so does the function

$$z_i = \int_0^z \omega_j(z)\, dz$$

since $P(z)$ now becomes

$$P(z) \to (z - a_i)^2 \prod_{j=1}^{(2k+1)} (z - a_j)$$

with $j \neq 1, i + 1$.

One technical point to note is that the expression for $\omega_i(z)dz$ written down in terms of the hyperelliptic function needs to be normalized before it can be used in the Theta Function.

The general structure of such a meromorphic function $f(w)$ is now

$$f(w) = \alpha \prod_{i=1}^{(k+1)} \frac{w - w_{a_i}}{w - w_{b_i}}$$

With a local parameter

$$k_a(w_a) = f(w) - f(w_a)$$

where we also require that

$$f(w_{u_k}) = f(w_{v_k})$$

This requirement comes from a global constraint that the distortion parameters have to satisfy. With these variables we can explicitly identify the parameters. These parameters describe the nature of distortions and carry information about the network because they contain the location of the pinch points and deformed period matrix.

For our case $w_a = w_{a_{k+1}}, w_b = w_{a_j}$. We have

$$V_{a,k} = \frac{1}{k_a'(w_a)} \left[ \frac{1}{w_a - w_b} - \frac{1}{w_a - w_{u_k}} \right]$$

$$W_{a,k} = A_{a,k} + B_{a,k}$$

$$A_{a,k} = \frac{1}{k_a'(w_a)^2} \left[ - \frac{1}{\left(w_a - w_{v_k}\right)^2 + \left(\frac{1}{w_a - w_{u_k}}\right)^2} \right]$$

$$B_{a,k} = - \frac{k_a''(w_a)}{k_a'(w_a)^2} V_{a,k}$$

where $V_{a,k}, W_{a,k}$ are pinch deformation functions. Then the Theta Function becomes

$$e^{\left[\sum_{i,k=1}^{k+1} (i\pi\Omega)_{ik} \alpha_i \alpha_k + \sum_{k=1}^{k+1} 2i\pi\alpha_k z_k\right]} = det(T)$$

$$(T)_{ik} = \delta_{ik} + \frac{w_i - s_i}{w_k - s_k} e^{z_i + z_k}$$

where each characteristic $\alpha_i,\ i = 1, 2, \cdots k$ can only be 0 or $^1/_2$ and

$$z_i^j = Z_i - d_i + \beta r_{j,i}$$

$$Z_i = iV_{a_{k+1},i}x + iW_{a_{k+1},i}t$$

while

$$r_{j,k} = \ln \frac{\left[\left(w_{a_j} - w_{v_k}\right)\left(w_{a_{k+1}} - w_{u_k}\right)\right]}{\left[\left(w_{a_j} - w_{u_k}\right)\left(w_{a_{k+1}} - w_{v_k}\right)\right]}$$

and $\beta$ is a constant that can take values (-1, 0, +1) while the parameters $d_k$ are constant for the pair of points $(a_j, b_j)$ that come together under pinch deformation.

In terms of these variables the dark soliton $\psi_j(x,t), 1 \leq j \leq k$ solution[4] of the non-linear Schrödinger equation can be written as,

$$\psi_j(x,t) = A_j e^{i\pi W} \frac{det\left(T_{j,1}\right)}{det\left(T_{j,0}\right)} e^{-i\left(E_j x - F_j t\right)}$$

where $A_j, E_j, F_j$ are known constants[4]. The soliton variables depend on the parameters $(w_i - s_i)$ and the variables $z_i$, that explicitly depend on the deformation parameters $V_{a,k}, W_{a,k}$ while the set of non-zero characteristics carry information about the network responsible for generating the signal. The deformed period matrix also appears in the solutions. The phase $\theta$ is the topological phase.

$$W = 4\sum_{i=1}^{k} \alpha_i \beta_i$$

where *W* is the topological parameter associated with spin structure and that there are *k* pulses if the system has *k* pinches. Besides these topological parameters the solution also carries the geometrical details regarding the nature of pinch deformations with them.

**VIII.A** Helical magnetic trace and spin structure formation

We established (App.IV B) that is theoretically possible to determine the voltage profile $\psi_j(z,t)$ of the $j^{th}$ moving soliton pulse in a train of *N* solitons, at a point *z* of the center line of a tube of the network by solving the nonlinear Schrödinger equation. We now want to determine the surface magnetic field generated by these pulses as they move along a network tube. The first step is to replace the voltages by equivalent charge densities. This is done by using Poisson's equation[9] of electromagnetic theory. Thus, we replace the voltage potential by its equivalent charge distribution $\rho(z,t)$, given by,

$$\frac{d^2\psi_j(z,t)}{dz^2} = 2\rho(z,t)$$

Further simplifications are made. The expression for the charge density $\rho(z,t)$ is next written as

$$\rho(z,t) = \frac{Q(z,t)}{\Delta_j} = \frac{N_j e v_j}{\Delta_j}$$

where $\Delta_j$ is the effective width of the soliton pulse and we have written $Q_j$ as

$$Q_j(z,t) = N_j e v_j$$

where *e* is the charge of an electron, so that $N_j e$ is the equivalent soliton charge at the point *z*. These simplifications will allow us to clearly link the way the transient magnetic field of the soliton pulses voltage produce a static helical spin magnet structure.

The transient helical surface magnetic field by a moving pulse, in the approximation described[9] is given by

$$B_j(z) = \frac{N_j e v}{c r_a^2}$$

where *c* is the velocity of light in the medium an $r_a$ is the radius of the tube surrounding the moving charges. We use cgs units for our calculations. We can estimate B to be $B \approx N_j 10^{-8}$ Gauss, using $c \approx 10^9$ cm/s [10], $e \approx 10^{-10}$ , $r \approx 10^{-4}$, $v_j \approx 10^3$ cm/s. The last to values ($r$ and $v_j$) are examples chosen to be biologically relevant by emulating axonal radius and action potential speed[11]. If the surface tube is considered to have thickness, then two such transient magnetic fields on the two surfaces, of radii $r_\pm$ will be generated with helical magnetic structures,

$$h(z,r_\pm) = B_j(z,r_\pm)\left[\cos\left(\frac{2\pi z}{r_\pm}\right), \sin\left(\frac{2\pi z}{r_\pm}\right)\right], z = v_j t$$

*N* multi soliton pulses will generate a sequence of transient magnetic fields

$$B(z) = \sum\nolimits_{j=1} N B_j(z)$$

Static magnetic structures are created by the transient magnetic field by aligning surface spins $s_i(z),\ i = 1,2$. These structures capture the helical nature of the transient magnetic surface field created and thus contain a magnetic trace of the parameters carried by the soliton pulses.

For a train of soliton pulses with slightly different velocities the excitation frequencies for the helical trace would be a band of frequencies. A simple representation of the transient magnetic helical curve can be written as

$$B(t) = (B\cos(\omega t)\,, B\sin(\omega t)\,, \omega t)$$

which then could be plotted for two values of the tube radii $r_{\pm}$ to emulate the theoretical thickness of the tube.

We determine the static spin structure created by the transient magnetic field of the solitons in the next section and show that they have a natural excitation frequency. The structure formed has to be preserved by the electron spin magnet interactions if it is to create a trace that can be thermodynamically stable in time.

The helical spin structure is a magnetic structure but has no macroscopic magnetic properties. This is because of a special topological property of spins, namely they reverse their orientation after a rotation of $2\pi$. This means that neighboring spins on the helix have opposite orientations. They pair to form units that have no magnetic property and have zero spin, that naturally form coherent structures which respond to thermal disruption as a single unit. The temperature stability of this structure, with *N* spin pairs requires

$$\frac{N\mu^2}{r^3} > kT$$

where $\mu$ is Bohr magnetron, *r* the distance between a spin pair, *k* the Boltzmann constant, and *T* the temperature in Kelvins.

**VIII.B** Spin Magnet Structure and its Frequency

We next determine the spin-magnet surface structure and its excitation frequency.

We first estimate the frequency associated with the interaction of this helical field with surface electron spin magnets by using a quantum theory formula, since the dynamical behavior of electron is governed by quantum ideas. The quantum interaction of the electron spin with an external magnetic field is given by

$$H = \mu_e \vec{B}.\vec{\sigma}$$

where $\vec{\sigma}$ are Pauli spin matrices, and $\mu_e = 2\mu$ where $\mu$ is the Bohr magneton. The Pauli matrices are operators that are used to describe the electron magnetic spin states.

Quantum theory tells us that the interaction energy $H$ has a natural excitation frequency given by

$$\omega = \frac{H}{\bar{h}}$$

We estimate this frequency by using the previous estimate for *B* and replacing $\vec{B}.\vec{\sigma}$ by $\frac{1}{2}B$. This replacement indicates that the spin is aligned to the magnetic field. Then

$$\omega = \frac{\mu B}{\bar{h}} = \frac{10^{-19}x10^{-8}}{10^{-27}} \approx 1$$

where we set $\mu \approx 10^{-19}$ , $\bar{h} \approx 10^{-27}$ in cgs units. Thus, for a pulse carrying $N_j$ units of electron charge, in the range $1 \leq N_j \leq 10^2$, will lead to the excitation frequencies of the static magnetic trace to be in the range $1 \leq \omega_j \leq 100$ Hz, for our estimations.

We next determine the static helical spin magnet structure. A quantum calculation is needed to do this. The time evolution of a spin is described by the operator

$$U(t) = e^{-i\frac{Ht}{\bar{h}}}$$

where

$$H = \mu\vec{B}.\vec{\sigma} = \mu\vec{\hat{n}}.\vec{\sigma}B$$

where we have written

$$\vec{B} = \vec{\hat{n}}B$$

and $\vec{\hat{n}}$ is the direction of the magnetic field $\vec{B}$. We now use the identity

$$e^{-i\left(\frac{\mu}{v_j\bar{h}}\right)\vec{\hat{n}}.\vec{\sigma}Bt} = \cos\left[\frac{\mu}{v_j\bar{h}}\vec{\hat{n}}Bt\right] - i\vec{\hat{n}}.\vec{\sigma}\sin\left[\frac{\mu}{v_j\bar{h}}\vec{\hat{n}}Bt\right]$$

The time evolution of an initial spin $S_j(0)$ in quantum mechanics is given by

$$S_j(t) = e^{-i\frac{Ht}{\bar{h}}}S_j(0)$$

But in our case the electrons are fixed locations along the path of the transient magnetic field and the only effect of the transient magnetic field is to align the spins at different locations it interacts with. Thus, we need to study the distributions of spins present in the helical pathway of the transient field. To do so we replace $t$ by $t = \frac{z}{v_j}$, where $z$ is a surface point in the pathway of the transient magnetic field. The appropriate spatial spin aligning evolution operator is $U(z)$, given by,

$$U_j(z) = e^{-i\left(\frac{\mu}{v_j}\right)\vec{B}.\vec{\sigma}z} = \cos\left[\left(\frac{\mu}{v_j\bar{h}}\right)Bz\right] - i\vec{\sigma}.\vec{\hat{n}}\sin\left[\left(\frac{\mu}{v_j\bar{h}}\right)Bz\right], 0 \leq z \leq L$$

We next write $\vec{\sigma}.\vec{\hat{n}} = \frac{1}{2}$ which is the aligned spin value projected out by the evolution operator. Thus, our static helical spin-magnet distribution $S_j(z)$ is given by,

$$S_j(z) = \left(\cos\left[\left(\frac{\mu}{v_j\bar{h}}\right)Bz_j\right] - i\sin\left[\left(\frac{\mu}{v_j\bar{h}}\right)Bz_j\right]\right)S_j(0), \qquad 0 \leq z_j \leq L$$

where $S_j(0)$ is the spin value at $z = 0$. It is a helical chain of electron spin magnets. The structure has no net macroscopic magnetic moment. We have already pointed out that the structure would have a natural excitation frequency. For $g$ pulses there will be $g$ static structures given by

$$S(z) = \sum_{j=1}^{g} S_j z_j$$

The corresponding structure will have a greater value for its magnetic strengt

**Figure S1.**

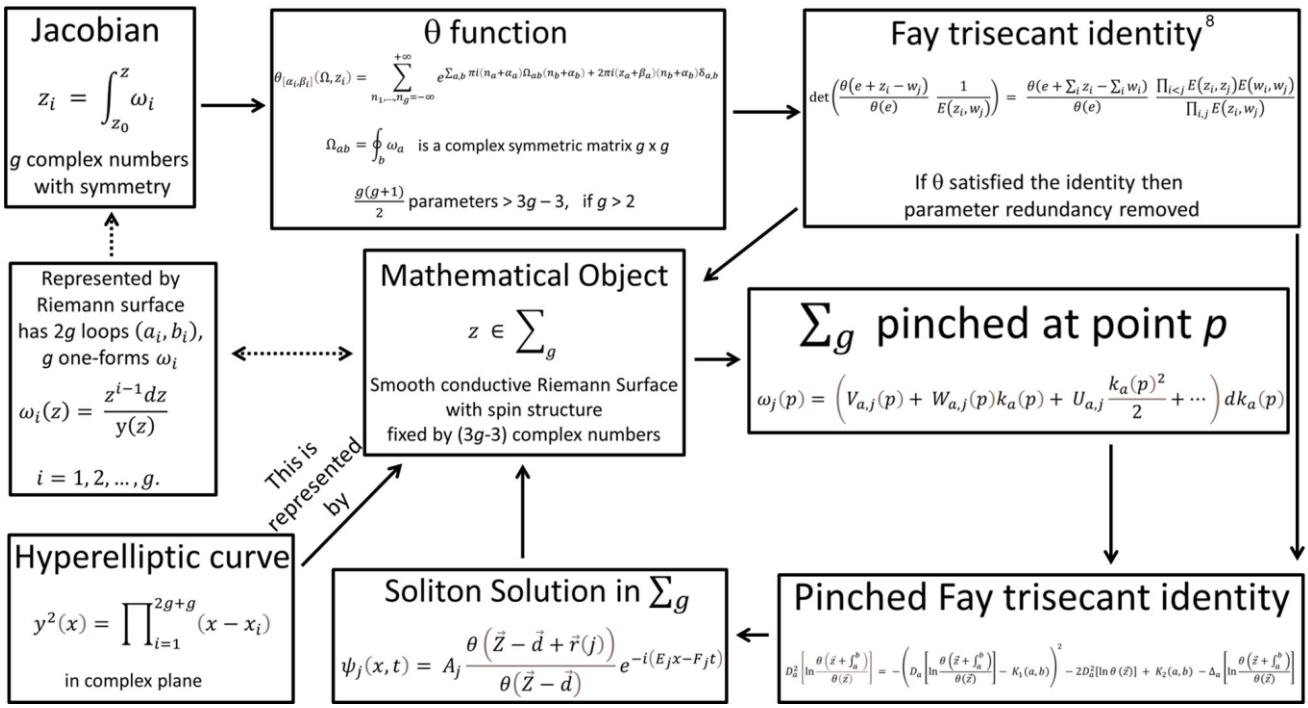


**Figure S1**: Mathematical diagram of the conceptual interactions that conform the presented framework, the interaction of them through the dynamical law that allows us to solve it generating soliton solutions.

**SI References**


45. Teleman, C., ”Riemann Surfaces. Lent Lectures.” (Berkeley Math 2003)
46. Munkres, J., “Topology. Pearson New International Edition.” (Pearson 2014)
47. Mumford, D., “Tata Lectures on Theta II.” (Brikhäuser 1984)
48. Kalla, C., New degeneration of Fay’s identity and its application to integrable systems. *International Mathematics Research Notices* 2013: 4170-4222 (2012)
49. Belokolos, E. D., “Algebro-geometric Approach to Nonlinear Integrable Equations, Springer Series in Non-linear Dynamics.” (Springer-Verlag 1994)
50. Feinberg, G. and Sucher, J., General theory of the van del Waals interaction: a model-independent approach. *Physical Review A* 2: 2395 (1970)
51. Fay, J.D., “Theta functions on Riemann Surfaces.” Lecture Notes in Mathematic 352. (Springer-Nature 1973)
52. Sen, S. and Raina, A.K., Grassmannians, multiplicative ward identities and theta-function identities. *Physics Letters B* 203: 256-262 (1988)
53. Jackson, J.D., “Classical Electrodynamics.” (John Wiley & Sons, Inc. 1999)
54. Khurgin, J., Slow light in various media: a tutorial. *Advances in Optics and Photonics* 2(3): 287-318 (2010)
55. Scott, A., “Neuroscience: A Mathematical Primer.” (Springer-Verlag 2002)